JCTC Journal of Chemical Theory and Computation

Geometries of Second-Row Transition-Metal Complexes from Density-Functional Theory

Mark P. Waller,[†] Heiko Braun,[‡] Nils Hojdis,[‡] and Michael Bühl*,[†]

Max-Planck-Institut für Kohlenforschung, Kaiser-Wilhelm-Platz 1, D-45470 Mülheim an der Ruhr, Germany, and Bergische Universität Wuppertal, Fachbereich Mathematik und Naturwissenschaften, D-42097 Wuppertal, Germany

Received July 19, 2007

Abstract: A data set of 19 second-row transition-metal complexes has been collated from sufficiently precise gas-phase electron-diffraction experiments and used for evaluating errors in DFT optimized geometries. Equilibrium geometries have been computed using 15 different combinations of exchange-correlation functionals in conjunction with up to three different effective core potentials. Most DFT levels beyond the local density approximation can reproduce the 29 metal−ligand bond distances selected in this set with reasonable accuracy and precision, as assessed by the mean and standard deviations of optimized vs experimentally observed bond lengths. The pure GGAs tested in this study all have larger standard deviations than their corresponding hybrid variants. In contrast to previous findings for first-row transition-metal complexes, the TPSSh hybrid meta-GGA is slightly inferior to the best hybrid GGAs. The ranking of some popular density functionals, for second-row transition-metal complexes, ordered according to decreasing standard deviation, is VSXC ≈ LSDA > BLYP > BP86 > B3LYP ≈ TPSSh > PBE hybrid ≈ B3PW91 ≈ B3P86. When zero-point vibrational corrections, computed at the BP86/SDD level, are added to equilibrium bond distances obtained from a number of density-functional/basis-set combinations, the overall performance in terms of mean and standard deviations from experiment is not improved. For a combined data set comprised of the first- and second-row transition-metal complexes the hybrid functionals B3P86, B3PW91, and the meta-GGA hybrid TPSSh afford the lowest standard deviations.

Introduction

More than 40 years after the birth of modern density functional theory (DFT) the exact exchange-correlation functional remains ever elusive. Therefore DFT currently employs a heuristic approach, spawning an extraordinarily large number of approximate functionals being proposed in the literature. As DFT remains reliant upon judicious validation against experiment (i.e., parametrization), accurate experimental data is vital, and the quality of a particular functional is ultimately connected to the quality of experimental data available. A growing body of literature for a posteriori estimates of errors for particular exchange-correlation functionals forms the basis for critical assessment of conclusions drawn from computational results within a DFT framework.

It is particularly important to evaluate the quality of DFT-derived geometries, as their accuracy may be crucial for further computations of energies or properties. For the important class of transition-metal complexes (a stronghold of modern DFT) this validation is hampered by a scarcity of accurate structure determinations in the gas phase, to which the overwhelming majority of DFT applications would refer. Quite frequently, parameters optimized for pristine molecules are compared to those obtained from X-ray crystallography or neutron diffraction, that is, for structures

* Corresponding author fax: + (0)208-306 2996; e-mail: buehl@mpi-muelheim.mpg.de.

[†] Max-Planck-Institut für Kohlenforschung.

[‡] Universität Wuppertal.

10.1021/ct700178y CCC: $37.00
Published on Web 10/19/2007

Chart 1. Data Set 2: Second-Row Transition-Metal Complexes

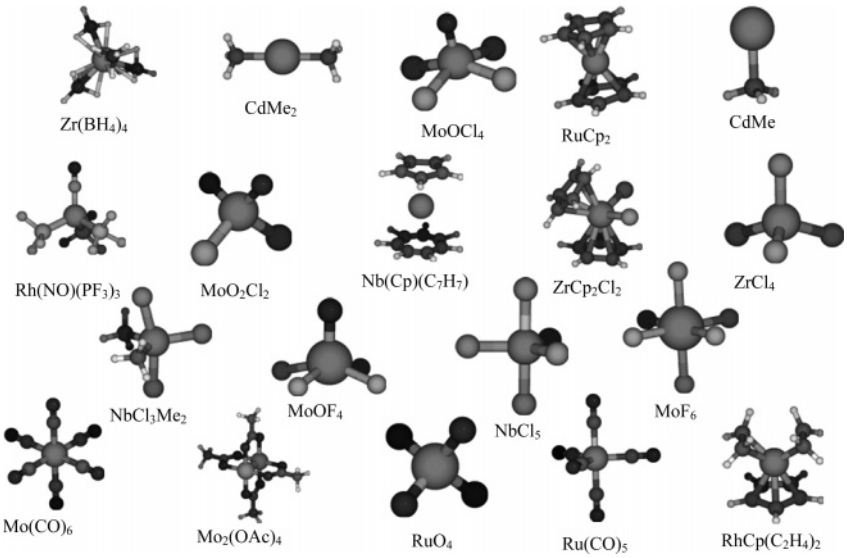

in the solid with unknown effects from packing forces and intermolecular interactions.

Occasionally, newly developed functionals are also tested against gas-phase geometries but usually only for a small number of complexes (see refs 1−6 for a few illustrative examples). The overall experience with DFT-optimized geometries is that most gradient-corrected (GGA) or hybrid functionals perform reasonably well, albeit with a tendency to overestimate metal−ligand bond distances by several pm, and with deviations typically increasing from metal−C to metal−P bonds.[7] We recently published a study evaluating the ability of DFT to reproduce experimental gas-phase geometries for a test set containing complexes from the first transition row, hereafter paper 1.[8] This study assessed popular density functionals and basis sets in terms of mean and standard deviations between optimized and experimental metal−ligand bond lengths in the gas phase. Drawing from a large compilation of gas-phase structures, from gas-phase electron diffraction (GED) and/or microwave spectroscopy (MW), we proposed a data set comprised of first-row transition-metal complexes. This data set is now referred to as data set 1, encompassing complexes of all 3d metals from Sc to Cu. Only metal−ligand bond lengths that have been determined with a precision better than 1 pm were incorporated, affording a test set of 32 molecules with 50 individual bond distances. Statistical analysis allowed the ranking of a number of popular functionals according to mean and standard deviations from experiment over all these distances.

The comparison between experimental and optimized bond lengths is hampered by the fact that the former refer to thermally averaged quantities, whereas the latter are equilibrium values, i.e., pertaining to vibrationless entities at 0 K.[9] Even if the experiments could be conducted at (or extrapolated to) that temperature, they would still yield structures averaged over the zero-point motion (r_g^0) and could not be directly compared to equilibrium geometries (r_e) from simple energy minimization. There is evidence for small first-row molecules that the zero-point motion actually affords the largest correction to equilibrium distances and that thermal effects on top of them (i.e., the difference between zero and finite T) tend to be much smaller.[10] If this holds also for the transition-metal complexes, computed zero-point corrected geometries would be much better suited for direct comparison with experiment than the raw equilibrium structures.

In a follow-up study for data set 1, we applied vibrational corrections to the equilibrium geometries,[11] using two perturbation methods that have been devised to compute such corrections.[12,13] The standard deviations were not reduced, however, and the relative ordering of functionals did not change with the addition of such vibrational corrections.

We now extend these studies to compounds from the second transition row. In an analogous fashion to data set 1, we selected data set 2 comprising sufficiently precise distances (again better than 1 pm) that have been determined experimentally at room temperature or slightly above (see Chart 1). In many cases, not all degrees of freedom have been refined experimentally, and only mean values for formally nonequivalent distances are known. The final selected experimental parameters are collected in Table 1. Data set 2 does have some notable absences, namely, no complexes containing yttrium, technetium, or silver and, perhaps most unfortunate, no palladium containing complexes. Although with just 19 molecules and 29 bonds, data set 2 is smaller than data set 1, the molecules collated in data set 2 should provide some insight into the relative performance of different density functionals for second-row transition-metal complexes. A number of popular local, gradient-corrected, hybrid, and meta-GGA functionals, together with a variety of effective core potentials (ECPs) and basis sets, are assessed in terms of mean and standard deviation from the corresponding experimental reference values for data set 2, in an analogous fashion to paper 1. We also report computed zero-point corrections to the bond distances for data set 2 in order to furnish increments to estimate r_g^0 from r_e values, thus facilitating the comparison between theory and experiment.

The broad aims of this paper are twofold: first, it is directed toward the identification of functionals, which perform well in terms of optimized geometry, specifically

Table 1. Bond Lengths *r* (in pm) of Second-Row Transition-Metal Complexes in the Gas Phase, as Derived by GED,[a] and Vibrational Corrections Δr_{vib} to Equilibrium Values, Computed at the BP86/SDD Level

ref	compd *symmetry*	parameter	[bond no.][b]	$r_{a/g}$	Δr_{vib}
39	$ZrCl_4$ T_d	*r*(Zr−Cl)	[1]	232.8(5)	0.18
40	$Zr(BH_4)_4$ *T*	*r*(Zr-B)	[2]	232.4(5)	2.74
		$r(Zr-H^{br})$	[3]	214.4(6)	3.22
41	$ZrCp_2Cl_2$ C_2	$r(Zr\text{-}C)^{mean}$	[4]	249.2(9)	1.08
42	$NbCl_5$ D_{3h}	$r(Nb-Cl^{ax})$	[5]	230.6(5)	0.26
		$r(Nb-Cl^{eq})$	[6]	227.5(4)	0.21
43	$NbCl_3Me_2$ C_{2v}	$r(Nb-Cl^{ax})$	[7]	230.4(5)	0.37
		$r(Nb-Cl^{eq})$	[8]	228.8(4)	0.59
		r(Nb-C)	[9]	213.5(9)	0.11
44	$Nb(Cp)(C_7H_7)$ C_s	$r(Nb\text{-}C)^{mean\ c}$	[10]	235.8(2)	0.45
45	MoF_6 O_h	*r*(Mo−F)	[11]	182.0(3)	0.17
46	$MoOF_4$ C_{4v}	*r*(Mo═O)	[12]	165.0(7)	0.23
		r(Mo−F)	[13]	183.6(3)	0.17
46	$MoOCl_4$ C_{4v}	*r*(Mo═O)	[14]	165.8(5)	0.01
		r(Mo-Cl)	[15]	227.9(3)	0.29
47	MoO_2Cl_2 C_{2v}	*r*(Mo═O)	[16]	168.6(4)	0.12
		r(Mo-Cl)	[17]	225.8(3)	0.32
48	$Mo_2(OAc)_4$ C_4	$r(Mo\overset{4}{-}Mo)$	[18]	207.9(3)	0.26
		r(Mo−O)	[19]	210.8(3)	0.35
49	$Mo(CO)_6$ O_h	*r*(Mo−C)	[20]	206.3(3)	0.46
50	RuO_4 T_d	*r*(Ru═O)	[21]	170.6(3)	0.30
51	$Ru(CO)_5$ D_{3h}	$r(Ru-C^{ax})$	[22]	195.0(9)	0.42
		$r(Ru-C^{eq})$	[23]	196.9(3)	0.45
52	$RuCp_2$ D_{5h}	*r*(Ru-C)	[24]	219.6(3)	0.59
53	$Rh(NO)(PF_3)_3$ C_3	*r*(Rh-P)	[25]	224.5(5)	1.00
54	$RhCp(C_2H_4)_2$ C_s	$r(Rh-C^{Cp})$	[26]	226.3(2)	0.87
		$r(Rh-C^{C2H4})$	[27]	210.9(2)	0.77
55	CdMe C_{3v}	$r(Cd\text{-}C)^{d}$	[28]	222.1(7)	2.01
56	$CdMe_2$ D_3	*r*(Cd-C)	[29]	211.2(4)	0.45

[a] br = bridging, Cp = cyclopentadienyl, ax = axial, eq = equatorial, Me = methyl, OAc = acetate. [b] In brackets: running number of bonds. [c] Doublet ground state. [d] $^2A_1$ state.

for second row-transition-metal complexes; second, we present a combined set of 3d- and 4d-transition-metal complexes in order to assess the performance of functionals over a more diverse range. The consequences of such analysis should serve to assist future DFT studies in preselecting candidate functionals for further more rigorous and system-specific validation. Furthermore, the data set may be useful for the future refinements of density functionals in order to attain better performance for transition-metal complexes.

Computational Details

Geometries were fully optimized in the given symmetry (as given in Table 1) using Gaussian 03[14]and several local (LSDA)[15] and gradient-corrected density functional combinations as implemented therein. Most functionals are composed of one of several exchange parts, namely Becke (B),[16] Becke hybrid (B3),[17] OPTX(O),[18] or OPTX hybrid (O3),[19] together with one of several correlation parts, namely P86,[20] PW91,[21] or LYP[22] (in parentheses: symbols used in combined forms). Other functionals comprise HCTH/407 (denoted HCTH)[3,23] and the PBE hybrid functional[24] (denoted PBE1, Gaussian keyword PBE1PBE) as well as the meta-GGAs BMK,[25] VSXC,[26] TPSS,[27] and TPSS hybrid (denoted TPSSh).[28] A fine integration grid (75 radial shells with 302 angular points per shell) has been used, except for VSXC, which has been shown to require finer grids[29] (here we used 99 radial shells with 590 angular points). The following relativistic small-core ECPs with the corresponding valence basis sets were employed on the metals: LANL2DZ[30] (with [3s3p2d] valence basis), SDD,[31] i.e., the Stuttgart-Dresden ECP (together with the [6s5p3d] valence basis), and CEP-121G (with a [4s4p3d] valence basis).[32] On the ligands, the 6-31G* basis[33] was used throughout, except for the selected cases, where Dunning's double-ζ basis[34] was used on the ligands. In addition, we tested Ahlrichs-type valence basis sets that had been designed for the use with the SDD ECPs,[35] denoted svp, tzvp, and qzvp (with [5s3p2d1f], [6s4p3d1f], and [7s5p4d3f1g] contractions for the metals, respectively), together with the corresponding all-electron bases on the ligands.[36−38] For essentially all combinations of functionals, ECPs, and ligand basis sets, the minimum character of all optimized structures was verified by evaluation of the harmonic vibrational frequencies. Closed- and open-shell species were treated with restricted and unrestricted formalisms, respectively. For the computation of effective geometries via the cubic force field, the Barone method[13] was invoked at the BP86/SDD level within Gaussian 03 revision D.01.[14] The default values were used for step size in the numerical differentiation (0.025 Å) and integration grid (SG1).

Results and Discussion

Equilibrium Bond Lengths. The 29 selected experimental metal−ligand bond distances (mostly r_a and r_g values from GED) are collated in Table 1. In a first step, the corresponding equilibrium bond lengths (r_e), optimized at various levels of DFT, are directly compared to these experimental data. In this first assessment, the accuracy of DFT is investigated via statistical analysis of the error, where this error is defined as r_e-r_{exp}, i.e., a positive value indicates overestimation of the optimized distance compared to experiment. The mean signed and unsigned deviations are given in Table 2, for a number of popular density functionals, together with standard and maximum absolute deviations.

Even though the nature of theoretical and experimental distances is different, a number of conclusions can be drawn from Table 2:

1. Optimized bond distances are, on average, always overestimated (cf. $\bar{\Delta}^{equil}$ values), except with LSDA, which, due to its significant overbinding, produces bond lengths shorter than refined from experiment. This was also clearly observed for data set 1 and has been noted in numerous other studies. Therefore LSDA is not recommended for complexes containing either first- or second-row transition metals. The performance of the VSXC functional is also particularly poor.

2. In agreement with our previous finding for data set 1, the BP86 variant is a promising pure GGA functional in terms of mean and standard deviation, and BPW91 is found to be comparable. Therefore both of these functionals should prove useful in conjunction with the popular resolution of identity (RI) approximation that has been implemented in a

Table 2. Statistical Assessment of Equilibrium (r_e) Metal−Ligand Bond Distances Computed at a Number of Levels of Theory Relative to Experimentally Reported Values (r_{exp})[a]

entry	functional	basis set[b]	$\bar{\Delta}^{equil}$	$\lvert\bar{\Delta}\rvert^{equil}$	$\bar{\Delta}_{std}^{equil}$	Δ_{max}^{equil}
1	PBE1	SDD	0.23	1.26	1.65	4.46 [8]
2	B3P86	SDD	0.54	1.28	1.57	4.10 [4]
3	BP86	SDD	2.41	2.57	2.03	6.51 [4]
4	B3PW91	SDD	0.88	1.42	1.59	4.64 [4]
5	BPW91	SDD	2.33	2.52	2.00	6.35 [4]
6	TPSSh	SDD	1.39	1.79	1.84	4.37 [4]
7	TPSS	SDD	2.10	2.31	1.96	5.19 [4]
8	O3LYP	SDD	1.34	1.88	1.93	5.79 [4]
9	OLYP	SDD	2.13	2.48	2.19	6.86 [4]
10	B3LYP	SDD	2.52	2.63	1.97	7.12 [28]
11	BLYP	SDD	4.53	4.53	2.48	11.47 [28]
12	HCTH	SDD	1.83	2.35	2.49	9.25 [28]
13	BMK	SDD	1.64	2.10	2.11	6.07 [7]
14	VSXC	SDD	3.18	3.18	2.93	16.90 [28]
15	LSDA	SDD	−1.49	2.55	2.70	5.00 [18]
16	B3P86	CEP-121G	1.36	1.58	1.48	4.80 [8]
17	BP86	CEP-121G	3.29	3.29	1.89	6.65 [4]
18	B3P86	LANL2DZ	1.39	1.81	2.55	10.34 [28]
19	B3P86	LANL2DZ[c]	3.61	4.12	3.35	9.06 [28]
20	BP86	LANL2DZ	3.59	3.65	3.39	16.12 [28]
21	BP86	LANL2DZ[c]	5.59	5.76	3.96	14.53 [28]
22	B3P86	svp	−0.40	1.35	1.70	−3.68 [21]
23	BP86	svp	1.52	1.85	1.93	6.00 [28]
24	B3P86	tzvp	−0.38	1.53	1.83	3.55 [4]
25	BP86	tzvp	1.64	2.03	2.10	6.84 [28]
26	BP86	qzvp	1.09	1.65	1.91	5.93 [4]

[a] All units are in picometers. $\bar{\Delta}^{equil}$, $\lvert\bar{\Delta}\rvert^{equil}$, $\bar{\Delta}_{std}^{equil}$, and Δ_{max}^{equil} denote mean, mean absolute, standard, and maximum absolute deviations, respectively. In square brackets: bond numbers from Table 1 for which the maximum error occurs. [b] 6-31G* basis for the ligands, except where otherwise noted. [c] D95 for the ligands.

number of computational chemistry packages.[57] The BLYP and OLYP functionals however have relatively larger errors for data set 2 and are therefore not particularly recommended for geometry optimization of transition-metal complexes.

3. The hybrid functionals perform always better than the corresponding pure GGAs. This is an important point, considering the active research into adapting the RI-approximation to hybrid-GGAs.[58] B3LYP is somewhat inferior to PBE1, B3PW91, and B3P86.

4. The meta-GGAs are not necessarily outperforming the hybrid functionals (such as B3P86 or B3PW91), for example compare entries 2 and 6. This is in direct contrast to previous observations obtained from analysis of data set 1, where the meta-GGAs showed significant improvement over the hybrid-GGAs. Although again here, for data set 2, these functionals do have a low mean deviation and a low standard deviation.

5. The three tested ECPs show increasing mean and standard deviations in the order SDD < CEP-121G < LANL2DZ, both at BP86 and B3P86 levels of theory. Even though the discrimination between SDD and CEP-121G is not very pronounced, the former appears to be the ECP of choice for complexes from the second transition row. In keeping with the findings for data set 1, the LANL2DZ ECP, is found to be inadequate for data set 2, in particular when used with small basis sets on the ligands, and is therefore not recommended for use in geometry optimization of transition-metal complexes.

6. The basis sets employed on the ligands can affect the bond lengths in gas-phase optimization using DFT. In conjunction with the LANL2DZ ECP, the smaller D95 Dunning basis set instead of the more common 6-31G* basis set does result in significant deterioration of agreement between theory and experiment.

7. The difference between the Ahlrichs-type svp, tzvp, and qzvp bases, as assessed by MAD and SD, is rather small when employing the BP86 functional, (compare entries 23, 25, and 26). The difference between the BP86 and B3P86 functionals using a particular Alrichs-type basis set is significantly larger in comparison (e.g. entries 22 vs 23 or 24 vs 25). Despite the rather large size of the qzvp basis set, the results of Table 2 show that it does not necessarily outperform the SDD/6-31G* combination for this data set of second-row transition-metal complexes.

To provide a easy interpretation of the data in Table 2, normal distributions with the same mean and standard deviations are plotted for selected functionals (BP86, B3LYP, TPSS, and TPSSh together with SDD and 6-31G* basis) in Figure 1a. The different ECPs and basis sets (SDD, LANL2DZ, and LANL2DZ:D95) combined with the BP86 functional are plotted in Figure 2b. This nicely summarizes the ability of optimized geometries computed using DFT to reproduce experimentally reported bond lengths for second-row transition-metal complexes.

The mean deviation for the 15 functionals and 3 basis sets (as given in Table 2) averaged over all bonds containing a particular metal are provided in Figure 2, in order to highlight particular transition metals that are particularly challenging for DFT. The gross overestimation of the distances involving Cd can be traced back to the Cd−C bond in CdMe, which, apparently, poses a special problem for DFT (note that the largest Δ_{max} values in Table 2 refer to this bond). Bond lengths involving Ru are particularly well reproduced. The remaining deviations are all around 2−3 pm, DFT is typically overestimating the experimental bond lengths.

Alternatively the ability of DFT to reproduce experimental bond lengths can be subdivided based on the identity of the ligand atom directly coordinated to the metal center. Figure 3 shows the mean deviation over the same levels of theory in Table 2 for the different ligand atom types. For the bonds to hydrogen, boron, and phosphorus, with only one representative, no conclusions can be drawn. The metal−O and metal−C bond distances are around 1 and 2 pm, respectively, longer than experiment on average. The metal−F and metal−Cl distances are slightly worse being, on average, around 3 pm longer than experiment; therefore, complexes which contain a metal halogen bond are more challenging for DFT.

Vibrationally Averaged Bond Lengths. We commence this section with a brief summary of findings from our recently published study of vibrational corrections applied to first-row transition-metal complexes in paper 2:[11] (a) the vibrational corrections are essentially transferable among different density functional and basis set combinations; (b) the corrections are almost exclusively positive (i.e., elonga-

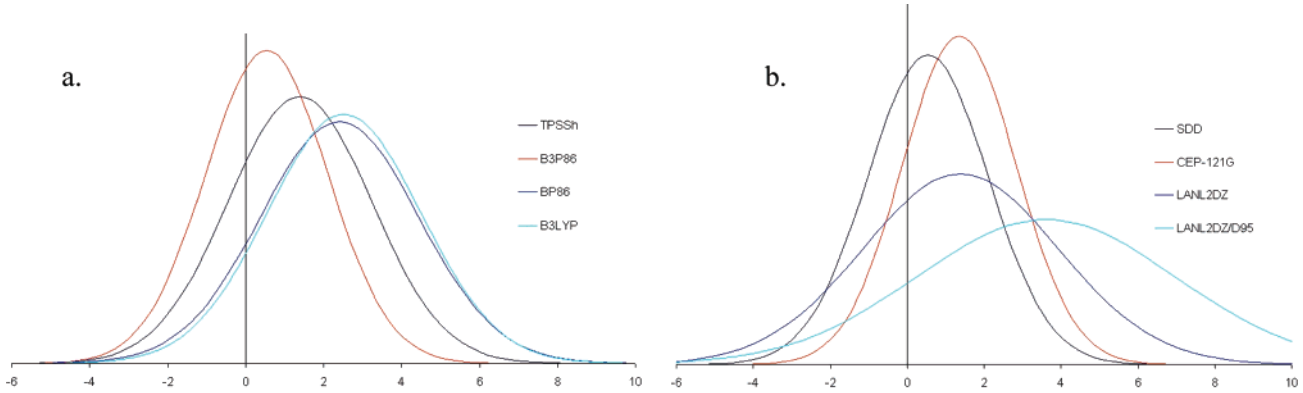

Figure 1. Normal distributions for the errors in the estimated metal−ligand bond lengths for data set 2: (a) displays the effects of different density functional using the SDD pseudopotential and (b) the ECP and basis-set dependence using the B3P86 functional (6-31G* on the ligand except where otherwise noted).

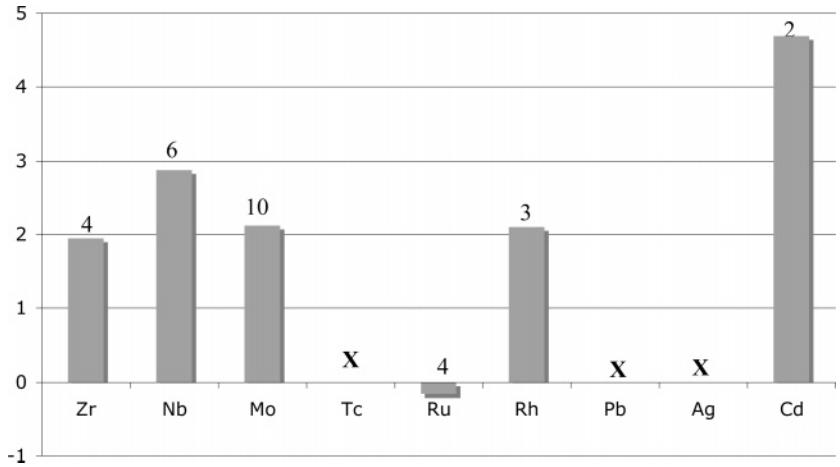

Figure 2. Mean deviation for different density functionals and basis sets combinations for complexes subdivided based on metal center, the number above the columns indicating the number of bonds containing the metal.

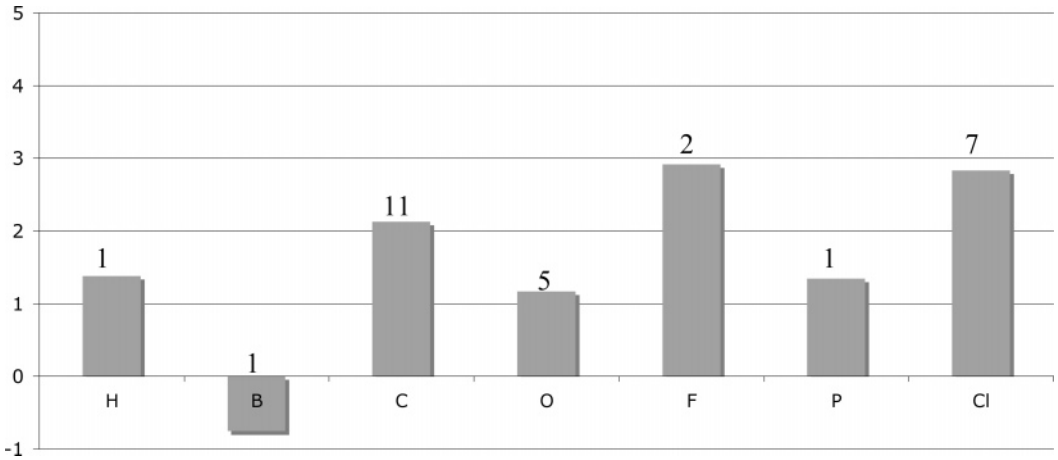

Figure 3. Mean deviation for different density functionals and basis sets combinations for bond lengths grouped according to coordinated ligand atom type, the number above columns indicating the number of bonds containing the element.

tion of equilibrium bond lengths); (c) the corrections do not reduce the standard deviation for data set 1 but simply increase the mean deviation (by ca. 0.5 pm).

For data set 2, the vibrational corrections obtained at the BP86/SDD level are collated in Table 1 (Δr_{vib} values), ranging essentially from zero ($MoOCl_4$: Mo═O) to ca. 2 pm (CdMe: Cd−C), i.e., similar in magnitude to those for data set 1. All effective metal−ligand bonds studied show an increase in bond length relative to the corresponding equilibrium structure, due to the anharmonicity of the potential energy surface. The mean deviation between effective and equilibrium bond lengths (i.e., the vibrational correction) amounts to 0.64 pm, which is 0.15 pm larger in magnitude than for the 3*d* transition-metal data set 1. In all but the LSDA case (using SDD/6-31G*) and the B3P86 functional (in conjunction with the Ahlrichs basis sets), all

Table 3. Statistical Assessment[a] of the Deviation between Estimated Effective Geometries (BP86/SDD Vibrational Correction Added to the Equilibrium Bond Lengths, Which Were Optimized at the Level of Theory Stated in Each Row) and Experimental Bond Lengths for Data Set 2 (Bond Lengths in pm)

entry	functional	basis set[b]	$\bar{\Delta}^{eff}$	$\lvert\bar{\Delta}\rvert^{eff}$	$\bar{\Delta}_{std}{}^{eff}$
1	PBE1	SDD	0.83	1.44	1.72
2	B3P86	SDD	1.19	1.55	1.57
3	BP86	SDD	3.02	3.13	1.99
4	B3PW91	SDD	1.45	1.71	1.62
5	BPW91	SDD	2.92	3.03	1.97
6	TPSSh	SDD	2.00	2.16	1.77
7	TPSS	SDD	2.57	2.74	1.99
8	O3LYP	SDD	1.94	2.23	2.01
9	OLYP	SDD	2.70	2.88	2.25
10	B3LYP	SDD	3.15	3.20	2.12
11	BLYP	SDD	5.02	5.02	2.69
12	HCTH	SDD	2.44	2.72	2.61
13	BMK	SDD	2.27	2.64	2.33
14	VSXC	SDD	3.49	3.74	3.55
15	LSDA	SDD	−0.78	2.26	2.58
16	B3P86	CEP-121G	2.00	2.02	1.45
17	BP86	CEP-121G	3.95	3.95	1.84
18	B3P86	LANL2DZ	2.12	2.36	2.68
19	B3P86	LANL2DZ[c]	4.08	4.47	3.55
20	BP86	LANL2DZ	4.18	4.21	3.53
21	BP86	LANL2DZ[c]	6.12	6.16	4.12
22	B3P86	svp	0.19	1.38	1.86
23	BP86	svp	2.10	2.30	2.08
24	B3P86	tzvp	0.21	1.54	1.97
25	BP86	tzvp	2.23	2.42	2.21
26	BP86	qzvp	1.66	1.98	2.00

[a] $\bar{\Delta}^{eff}$, $\lvert\bar{\Delta}\rvert^{eff}$, and $\bar{\Delta}_{std}{}^{eff}$ denote mean, mean absolute, and standard deviations, respectively. [b] 6-31G* for the ligands except otherwise stated. [c] D95 for the ligands.

errors in the equilibrium bond lengths were shown in the previous section to overestimate (to varying extent) experimental bond lengths on average. Therefore the agreement between effective geometries and experimentally refined gas-phase geometries in terms of mean and standard deviation is not improved.

In accord with the findings from data set 1, we assume transferability among functionals and use the vibrational corrections (Δr_{vib}) computed at the BP86/SDD level (Table 1) as increments, which are added to equilibrium bond lengths computed at a number of different levels of theory, affording a set of estimated effective geometries ($r^{est}{}_{eff} = r_e + \Delta r_{vib}$). In an analogous fashion to paper 2, effective bond lengths are assessed in terms of mean and standard deviations (Table 3). The key result from Table 3 is that applying vibrational corrections does not necessarily improve agreement between experiment and theory and, in fact, decreases agreement for all density functionals except with the LSDA/SDD/6-31G* and BP86/SDD/tzvp combinations. It appears that the vibrational corrections are simply shifting the error distribution in the positive direction without greatly affecting its width.

Combined Data Sets. The selection of a density functional for geometry optimization of molecules in the gas phase is clearly an important issue for computational chemistry. A functional with a narrow error distribution across a wider range of the periodic table is clearly advantageous. To aid in the selection of currently available functionals and to provide benchmarks for future development of functionals, analysis of data set 2 (second-row transition-metal complexes) is combined with the previous data set 1 (first-row transition-metal complexes) and is hereafter referred to as data set 3. As there appears to be no significant improvement between computed and experimentally observed bond lengths upon inclusion of vibrational effects into the theoretical calculations, we now focus on the raw equilibrium values. The corresponding statistical analysis of data set 3 is given in Table 4. The combined data set affords more general conclusions to be drawn regarding the accuracy and precision of modern DFT in transition-metal chemistry.

An overall ranking of functionals for the first- and second-row transition-metal complexes is however dominated by first-row complexes, as the first-row transition-metal complexes are over-represented in the combined data set (data set 3). In order to interpret Table 4 for the ranking of density functionals and basis sets based on their ability to reproduce experimental gas-phase geometries, we primarily consider the standard deviation. The convergence of the Alrichs-type basis sets is remarkably good for the combined data sets, compare entries 17−19, and these basis sets do significantly outperform both the 6-31G* and D95 basis sets, compare entries 2, 3, and 17−19, in conjunction with the BP86 functional. We crudely group the performance of functionals into three categories: not recommended, recommended, and highly recommended.

Not recommended: The LSDA and VSXC functionals again prove inadequate in providing reasonable geometries for first- and second-row transition-metal containing complexes. BLYP and OLYP are found to be inferior to other pure functionals tested within this study and therefore are also not recommended.

Recommended: The BP86 and BPW91 functionals perform comparatively well, and, therefore in cases where it is desirable to invoke the RI approximation, these functionals can be employed with only a marginally greater deviation from experiment, compared to their hybrid counterparts. These GGAs even perform slightly better than the popular B3LYP hybrid functional.

Highly recommended: B3P86, B3PW91, and TPSSh perform almost equally well in terms of standard deviation. The former two functionals are somewhat underestimating the experimental bond lengths (which would be improved upon inclusion of the zero-point corrections discussed above), and the hybrid meta-GGA is slightly overestimating. Therefore we conclude that these three functionals are highly recommended, as they appear most appropriate for geometry optimization of first- or second-row transition-metal complexes.

The normal distributions for three representative functionals are plotted in Figure 4. The normal distributions of a highly recommended (TPSSh), recommended (BP86), and nonrecommended (BLYP) functional provides a good visual indication of the performance.

Table 4. Statistical Assessment[a] of the Deviation between the Equilibrium Bond Lengths, Optimized at the Level of Theory Stated in Each Row, and Experimental Ones for Data Set 3 (Bond Lengths in pm)[b]

entry	functional	3d basis[c]	4d basis[c]	$\bar{\Delta}^{equil}$	$\lvert\bar{\Delta}\rvert^{equil}$	$\lvert\bar{\Delta}\rvert_{std}^{equil}$	$\lvert\Delta\rvert_{max}$
1	B3P86	AE1	SDD	−0.63	1.48	1.78	5.94 [I:35]
2	BP86	AE1	SDD	1.13	1.84	2.08	6.51 [II:4]
3	BP86	SDD	SDD	0.52	1.89	2.39	6.51 [II:4]
4	B3PW91	AE1	SDD	−0.26	1.47	1.81	5.61 [I:35]
5	BPW91	AE1	SDD	1.13	1.84	2.06	6.35 [II:4]
6	TPSSh	AE1	SDD	0.22	1.35	1.79	5.18 [II:8]
7	TPSS	AE1	SDD	0.88	1.54	1.89	5.96 [II:18]
8	O3LYP	AE1	SDD	0.28	1.70	2.07	5.79 [II:4]
9	OLYP	AE1	SDD	1.08	1.96	2.26	6.86 [II:4]
10	B3LYP	AE1	SDD	1.30	1.99	2.11	7.12 [II:28]
11	B3LYP	SDD	SDD	0.66	2.05	2.47	7.12 [II:28]
12	BLYP	AE1	SDD	3.16	3.23	2.42	11.47 [II:28]
13	HCTH	AE1	SDD	0.57	1.92	2.45	9.25 [II:28]
14	BMK	AE1	SDD	0.65	1.99	2.36	6.07 [II:7]
15	VSXC	AE1	SDD	2.19	2.34	2.37	16.90 [II:28]
16	LSDA	AE1	SDD	−2.92	3.32	2.54	9.46 [I:35]
17	BP86	svp	SDD/svp	0.30	1.68	2.11	6.00 [II:28]
18	BP86	tzvp	SDD/tzvp	0.87	1.74	2.05	6.84 [II:28]
19	BP86	qzvp	SDD/qzvp	0.41	1.49	1.87	5.14 [I:1]

[a] $\bar{\Delta}^{equil}$, $\lvert\bar{\Delta}\rvert^{equil}$, $\bar{\Delta}_{std}^{equil}$, and Δ_{max}^{equil} denote mean, mean absolute, standard, and maximum absolute deviations, respectively. [b] The corresponding mean and standard deviations for equilibrium bond lengths (uncorrected) are also shown for comparison. [c] 6-31G* for the ligands, unless otherwise stated. In square brackets: bond numbers from Table 1 in this paper or in paper 1 (labeled II and I, respectively), for which the maximum error occurs.

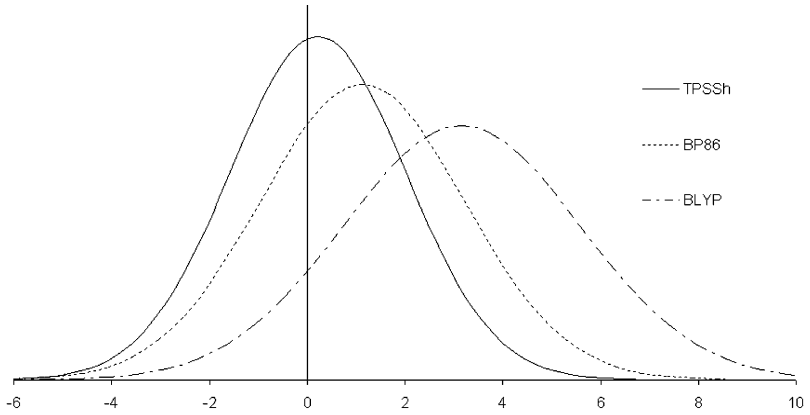

Figure 4. Normal distributions for the errors in the estimated metal−ligand bond lengths for data set 3, illustrating the effects of different density functionals in conjunction with the SDD ECP and 6-31G* basis set.

Conclusions

A new data set of 29 bond lengths comprised of second-row transition-metal complexes is proposed to be a good testing ground for existing density functionals and should be useful for validation of future density functionals or indeed for parametrization or reparametrization of hybrid functionals. Zero-point vibrational corrections (obtained at the BP86/SDD level) serve to increase equilibrium distances by ca. 0−2 pm, depending on the nature of the particular bond. Based on results obtained previously for 3d metals complexes, the vibrational corrections were transferred to the various density-functional/basis-set combinations to create estimated effective (vibrationally averaged) bond parameters. These corrections do not affect the widths of the error distributions (assessed as standard deviations between theoretical and experimental bond lengths) but simply shift these distributions to more positive values. As nearly all the functional trialed in this study on average overestimate the experimental bond lengths, this shift in bond length decreases agreement with experiment.

The combination of data set 2 which contains second-row transition-metal complexes present herein with the previous data set 1 (first-row transition-metal complexes) has created a larger more diverse set which should prove to be a useful testing suite for newly developed density functionals or ab initio methods, in order to assess the relative performance in reproducing the geometries of transition-metal complexes in the gas phase.

Acknowledgment. M.B. wishes to thank Prof. W. Thiel, the MPI Mülheim, and the Deutsche Forschungsgemeinschaft for continuing support. Computations were performed on a local computer cluster of Intel Xeon and Opteron PCs at the MPI Mülheim, maintained by Horst Lenk.

Supporting Information Available: Tables with individual optimized bond distances and BP86/SDD optimized Cartesian coordinates of all complexes. This material is available free of charge via the Internet at http://pubs.acs.org.

References

(1) Rosa, A.; Ehlers, A. W.; Baerends, E. J.; Snijders, J. C.; te Velde, G. J. *J. Phys. Chem.* **1996**, *100*, 5690−5696.

(2) Filatov, M.; Thiel, W. *Phys. Rev. A* **1998**, *57*, 189−199.

(3) Hamprecht, F. A.; Cohen, A. J.; Tozer, D. J.; Handy, N. C. *J. Chem. Phys.* **1998**, *109*, 6264−6271.

(4) (a) Schultz, N. E.; Zhao, Y.; Truhlar, D. G. *Phys. Chem. A* **2005**, *109*, 4388−4403. (b) Schultz, N. E.; Zhao Y.; Truhlar D. G. *Phys. Chem. A* **2005**, *109*, 11127−11143.

(5) Furche, F.; Perdew, J. P. *J. Chem. Phys.* **2006**, *124*, 044103.

(6) Neese, F.; Schwabe, T.; Grimme, S. *J. Chem. Phys*. **2007**, *126*, 124115.

(7) For example: Bray, M. R.; Deeth, R. J.; Paget, V. J.; Sheen, P. D. *Int. J. Quantum Chem.* **1997**, *61*, 85−87.

(8) Bühl, M.; Kabrede, H. *J. Chem. Theory Comput.* **2006**, *2*, 1282−1290.

(9) The equilibrium distance, r_e, is the distance between the positions of the nuclei on the potential energy surface, as obtained from standard geometry optimizations; r_g is the average internuclear distance at temperature T, r_g^0 that at zero K. It is the latter value that our computed effective geometries refer to. Typical quantities derived experimentally are r_a (the effective internuclear distance as derived from electron scattering intensity), r_α (the distance between average nuclear positions in the thermal equilibrium at temperature T), r_z (the distance between average nuclear positions in the ground vibrational state), or r_0 (the effective internuclear distance obtained from the rotational constants), see e.g.: Hargittai, I. In *Stereochemical Applications of Gas-Phase Electron Diffraction, Part A: The Electron Diffraction Technique*; Hargittai, I., Hargittai, M., Eds.; VCH Publisher: Weinheim, 1988; pp 1−54.

(10) Toyama, M.; Oka, T.; Morino, Y. *J. Mol. Spectrosc.* **1994**, *13*, 193−213.

(11) Waller, M. P.; Bühl, M. *J. Comput. Chem*. **2007**, *28*, 1531−1537.

(12) (a) Ruud, K.; Åstrand, P.-O.; Taylor, P. R. *J. Chem. Phys.* **2000**, *112*, 2668−2683. (b) Ruud, K.; Åstrand, P.-O.; Taylor, P. R. *J. Am. Chem. Soc.* **2000**, *123*, 4826−4833. (c) Ruden, T.; Lutnæss, O. B.; Helgaker, T. *J. Chem. Phys.* **2003**, *118*, 9572−9581.

(13) (a) Barone, V. *J. Chem. Phys.* **2004**, *120*, 3059−3065. (b) Barone, V. *J. Chem. Phys.* **2005**, *122*, 014108.

(14) Frisch, M. J.; Trucks, G. W.; Schlegel, H. B.; Scuseria, G. E.; Robb, M. A.; Cheeseman, J. R.; Montgomery, J. A., Jr.; Vreven, T.; Kudin, K. N.; Burant, J. C.; Millam, J. M.; Iyengar, S. S.; Tomasi, J.; Barone, V.; Mennucci, B.; Cossi, M.; Scalmani, G.; Rega, N.; Petersson, G. A.; Nakatsuji, H.; Hada, M.; Ehara, M.; Toyota, K.; Fukuda, R.; Hasegawa, J.; Ishida, M.; Nakajima, T.; Honda, Y.; Kitao, O.; Nakai, H.; Klene, M.; Li, X.; Knox, J. E.; Hratchian, H. P.; Cross, J. B.; Bakken, V.; Adamo, C.; Jaramillo, J.; Gomperts, R.; Stratmann, R. E.; Yazyev, O.; Austin, A. J.; Cammi, R.; Pomelli, C.; Ochterski, J. W.; Ayala, P. Y.; Morokuma, K.; Voth, G. A.; Salvador, P.; Dannenberg, J. J.; Zakrzewski, V. G.; Dapprich, S.; Daniels, A. D.; Strain, M. C.; Farkas, O.; Malick, D. K.; Rabuck, A. D.; Raghavachari, K.; Foresman, J. B.; Ortiz, J. V.; Cui, Q.; Baboul, A. G.; Clifford, S.; Cioslowski, J.; Stefanov, B. B.; Liu, G.; Liashenko, A.; Piskorz, P.; Komaromi, I.; Martin, R. L.; Fox, D. J.; Keith, T.; Al-Laham, M. A.; Peng, C. Y.; Nanayakkara, A.; Challacombe, M.; Gill, P. M. W.; Johnson, B.; Chen, W.; Wong, M. W.; Gonzalez, C.; Pople, J. A. *Gaussian 03, Revision D.01*; Gaussian, Inc.: Wallingford, CT, 2004.

(15) Vosko, S. H.; Wilk L.; Nusair, M. *Can. J. Phys*. **1980**, *58*, 1200−1211. Functional III of that paper used.

(16) Becke, A. D. *Phys. Rev. A* **1988**, *38*, 3098−3100.

(17) Becke, A. D. *J. Chem. Phys.* **1996**, *98*, 5648−5642.

(18) Handy, N. C.; Cohen, A. J. *Mol. Phys.* **2001**, *99*, 403−412.

(19) Cohen, A. J.; Handy, N. C. *Mol. Phys.* **2001**, *99*, 607−615.

(20) (a) Perdew, J. P. *Phys. Rev. B* **1986**, *33*, 8822−8824. (b) Perdew, J. P. *Phys. Rev. B* **1986**, *34*, 7406.

(21) (a) Perdew, J. P. In *Electronic Strucure of Solids;* Ziesche, P., Eischrig, H., Eds.; Akademie Verlag: Berlin, 1991. (b) Perdew, J. P.; Wang, Y. *Phys. Rev. B* **1992**, *45*, 13244−13249.

(22) Lee, C.; Yang, W.; Parr, R. G. *Phys. Rev. B* **1988**, *37*, 785−789.

(23) Boese, A. D.; Handy, N. C. *J. Chem. Phys.* **2001**, *114*, 5497−5503.

(24) (a) Perdew, J. P.; Burke, K.; Ernzerhof, M. *Phys. Rev. Lett.* **1996**, *77*, 3865−3868. (b) Perdew, J. P.; Burke, K.; Ernzerhof, M. *Phys. Rev. Lett.* **1997**, *78*, 1396. (c) Perdew, J. P.; Ernzerhof, M.; Burke, K. *J. Chem. Phys*. **1996**, *105*, 9982−9985. (d) Ernzerhof, M.; Scuseria, G. E. *J. Chem. Phys*. **1999**, *110*, 5029−5036.

(25) Boese, A. D.; Martin, J. M. L. *J. Chem. Phys.* **2004**, *121*, 3405−3416.

(26) Van Voorhis, T.; Scuseria, G. E. *J. Chem. Phys.* **1998**, *109*, 400−410.

(27) (a) Tao, J.; Perdew, J. P.; Staroverov V. N.; Scuseria, G. E. *Phys. Rev. Lett.* **2003**, *91*, 146401. (b) Tao, J.; Perdew, J. P.; Staroverov V. N.; Scuseria, G. E. *Phys. Rev. Lett.* **2004**, *120*, 6898−6911.

(28) (a) Staroverov, V. N.; Scuseria, G. E.; Tao, J.; Perdew, J. P. *J. Chem. Phys.* **2003**, *119*, 146401. (b) Staroverov, V. N.; Scuseria, G. E.; Tao J.; Perdew, J. P. *J. Chem. Phys.* **2004**, *121*, 11507.

(29) Johnson, E. R.; Wolkow, R. A.; DiLabio, G. A. *Chem. Phys. Lett*. **2004**, *394*, 334−338.

(30) Hay, P. J.; Wadt, W. R. *J. Chem. Phys.* **1985**, *82*, 299−310.

(31) Dolg, M.; Wedig, U.; Stoll, H.; Preuss, H. *J. Chem. Phys.* **1987**, *86*, 866.

(32) (a) Stevens, W.; Basch, H.; Krauss, J., *J. Chem. Phys.* **1984**, *81*, 6026. (b) Stevens, W. J.; Krauss, M.; Basch, H.; Jasien, P. G. *Can. J. Ch*em. **1992**, *70*, 612. (c) Cundari, T. R.; Stevens, W. J. *J. Chem. Phys.* **1993**, *98*, 5555.

(33) (a) Hehre, W. J.; Ditchfield, R.; Pople, J. A. *J. Chem. Phys.* **1972**, *56*, 2257−2261. (b) Hariharan, P. C.; Pople, J. A. *Theor. Chim. Acta* **1973**, *28*, 213−222.

(34) Dunning, T. H. In *Modern Theoretical Chemistry*; Schaefer, H. F., Ed.; Plenum Press: New York, 1977; Vol 4, pp 1−27.

(35) Weigend, F.; Ahlrichs, R. *Phys. Chem. Chem. Phys*. **2005**, *7*, 3297−3305.

(36) Schäfer, A.; Horn, H.; Ahlrichs, R. *J. Chem. Phys*. **1992**, *97*, 2571−2577.

(37) Schäfer, A.; Huber, C.; Ahlrichs, R. *J. Chem. Phys*. **1994**, *100*, 5829−5835.

(38) Weigend, F.; Furche, F.; Ahlrichs, R. *J. Chem. Phys*. **2003**, *119*, 12753−12762.

(39) Utkin, A. N.; Petrova, V. N.; Girichev, G. V.; Petrov, V. M. *Russ. J. Struct. Chem. (Engl. Transl.*) **1982**, *27*, 660−661.

(40) Haaland, A.; Shorokhov, D. J.; Tutukin, A. V.; Volden, H. V. *Inorg. Chem.* **2002**, *41*, 6646−6655.

(41) Ronova, I. A.; Alekseev, N. V. *Russ. J. Struct. Chem. (Engl. Transl.*) **1977**, *18*, 180−182.

(42) Gove, S. K.; Gropen, O.; Fægri, K.; Haaland, A.; Martinsen, K.-G.; Strand, T. G.; Volden, H. V.; Swang, O. *J. Mol. Struct*. **1999**, *485*−*486*, 115−119.

(43) (a) McGrady, S. G.; Haaland, A.; Verne, H. P.; Volden, H. V.; Downs, A. J.; Shorokhov, D.; Eickerling, G.; Scherer, W. *Chem. Eur. J*. **2005**, *11*, 4921−4934. Reinvestigation from the following: (b) Ischenko, A. A.; Strand, T. G.; Demidov, A. V.; Spiridonov, V. P. *J. Mol. Struct*. **1978**, *43*, 227−243.

(44) Mawhorter, R. J.; Rankin, D. W. H.; Robertson, H. E.; Green, M. L. H.; Scott, P. *Organometallics* **1994**, *13*, 2401−2404. Even though the mean bond length between Nb and the C atoms of the seven-membered ring is reported with an uncertainty below 1 pm in that paper, the difference between the mean Nb−C^{C7H7} and Nb−C^{C5H5} distances is associated with a much larger error. We therefore included the mean value over all Nb−C distances, which could be refined with the quoted precision.

(45) Seip, H. M.; Seip, R. *Acta Chem. Scand*. **1966**, *20*, 2698.

(46) Ijima, K. *Bull. Chem. Soc. Jpn*. **1977**, *50*, 373−375.

(47) Thomassen, H.; Hedberg, K. *J. Mol. Struct*. **1992**, *273*, 197−206.

(48) Kelley, M. H.; Fink, M. *J. Chem. Phys*. **1982**, *76*, 1407−1416.

(49) Seip, S. P.; Seip, H. M. *Acta Chem. Scand*. **1966**, *20*, 2711.

(50) Schäfer, L.; Seip, H. M. *Acta Chem. Scand*. **1967**, *21*, 737.

(51) Huang, J.; Hedberg, K.; Davis, H. B.; Pomeroy, R. K. *Inorg. Chem*. **1990**, *29*, 3923−3925.

(52) Haaland, A.; Nilsson, J. E. *Acta Chem. Scand*. **1968**, *22*, 2653−2670.

(53) Bridges, D. M.; Rankin, D. W. H.; Clement, D. A.; Nixon, J. F. *Acta Crystallogr., Sect. B: Struct. Sci*. **1972**, *B28*, 1130.

(54) Blom, R.; Rankin, D. W. H.; Robertson, H. E.; Perutz, R. N. *J. Chem. Soc., Dalton Trans.* **1993**, 1983−1986.

(55) Rotational spectroscopy from high-resolution laser-induced fluorescence spectra, r_0 value: Cerny, T. M.; Tan, X. Q.; Williamson, J. M.; Robles, E. S. J.; Ellis, A. M.; Miller, T. A. *J. Chem. Phys.* **1993**, *99*, 9376−9388.

(56) High-resolution Raman spectroscopy, r_0 value: Suryanarayana Rao, K.; Stoicheff, B. P.; Turner, R. *Can. J. Phys*. **1960**, *38*, 1516.

(57) (a) Dunlap, B. I. *J. Chem. Phys.* **1983**, *78*, 3140. (b) Dunlap, B. I. *J. Mol. Struct.* **2000**, *529*, 37. (c) Eichkorn, K.; Treutler, O.; Öhm, H.; Häser, M.; Ahlrichs, R. *Chem. Phys. Lett.* **1995**, *242*, 652−660.

(58) Weigend, F. *Phys. Chem. Cem. Phys.* **2002**, *4*, 4285−4291.

CT700178Y